

# A Distributed Hybrid Quantum Convolutional Neural Network for Medical Image Classification

Yangyang Li<sup>a,\*</sup>, Zhengya Qi<sup>a</sup>, Yuelin Li<sup>a</sup>, Haorui Yang<sup>a</sup>, Ronghua Shang<sup>a</sup>,  
Licheng Jiao<sup>a</sup>

*<sup>a</sup>Key Laboratory of Intelligent Perception and Image Understanding of Ministry of Education, Joint International Research Laboratory of Intelligent Perception and Computation, International Research Center for Intelligent Perception and Computation, Collaborative Innovation Center of Quantum Information of Shaanxi Province, School of Artificial Intelligence, Xidian University, No. 2 Taibai South Road, Yanta District, Xi'an, 710071, Shaanxi, China*

---

## Abstract

Medical images are characterized by intricate and complex features, requiring interpretation by physicians with medical knowledge and experience. Classical neural networks can reduce the workload of physicians, but can only handle these complex features to a limited extent. Theoretically, quantum computing can explore a broader parameter space with fewer parameters, but it is currently limited by the constraints of quantum hardware. Considering these factors, we propose a distributed hybrid quantum convolutional neural network based on quantum circuit splitting. This model leverages the advantages of quantum computing to effectively capture the complex features of medical images, enabling efficient classification even in resource-constrained environments. Our model employs a quantum convolutional neural network (QCNN) to extract high-dimensional features from medical images, thereby enhancing the model's expressive capability. By integrating distributed techniques based on quantum circuit splitting, the 8-qubit QCNN can be reconstructed using only 5 qubits. Experimental results demonstrate that our model achieves strong performance across 3 datasets for both binary and multiclass classification tasks. Furthermore, compared to recent technologies, our model achieves superior performance with fewer parameters, and

---

\*Corresponding author

*Email address:* [yyli@xidian.edu.cn](mailto:yyli@xidian.edu.cn) (Yangyang Li)

experimental results validate the effectiveness of our model.

*Keywords:* Medical image classification, Quantum convolutional neural network, Quantum circuit splitting, Distributed quantum computing

---

## 1. Introduction

Medical images play a crucial role in clinical diagnosis, characterized by intricate and complex features. Accurate interpretation of these images is imperative, as diagnostic outcomes directly influence patient treatment plans. However, this task demands a high level of medical expertise and extensive experience, imposing significant demands and workload on healthcare professionals.

To facilitate more efficient and accurate disease diagnosis while alleviating the workload of physicians, deep learning techniques have been incorporated into the field of medical image classification (Albahri et al. (2020)). Neural networks are effectively used to process these complex data, assisting in the extraction of valuable information and features, accelerating the processing and analysis of medical images, enhancing efficiency, and ultimately improving diagnostic accuracy and speed. However, models such as convolutional neural networks (CNNs)(Jiwani et al. (2022)), when processing large volumes of medical images, must increase model parameters and deepen network layers to extract more features, which inevitably increase the computational complexity of the network.

With the rapid advancement of quantum computing, quantum computers have demonstrated advantages in tackling challenging problems that are difficult for classical computers to solve (De Leon et al. (2021)). Leveraging quantum parallelism to swiftly process large volumes of medical data, the properties of quantum superposition and entanglement (Schuld et al. (2017)) enable more efficient high-dimensional data extraction using fewer quantum computing resources. To fully harness the acceleration advantages of quantum computing for real-world issues, certain requirements must be met regarding the quantity and quality of qubits.

Unfortunately, many of the quantum computing resources required for these technologies exceed the capabilities of today's quantum computers. The limitations of quantum computing hardware, particularly regarding entanglement operations and the number of logical qubits (Klimov et al. (2018)), have rendered distributed quantum computing an important strategy for address-

ing the problem of qubit expansion and achieving quantum advantage. However, research on distributed quantum neural networks is noticeably lacking and requires further development.

Based on the aforementioned background, a distributed hybrid quantum convolutional neural network is proposed. This approach aims to leverage the strengths of both quantum and classical computing to improve the efficiency and accuracy of medical image classification. By introducing specially designed a quantum convolutional neural network, it effectively extracts image features in multidimensional space. The distribution of the quantum neural network is achieved through quantum circuit splitting, which allows the required 8-qubit circuit to be reconstructed using a set of 4-qubit and 5-qubit circuits. This allows the execution of an 8-qubit QCNN using only a 5-qubit quantum computer, significantly reducing the spatial complexity of quantum computing and conserving quantum resources.

The main contributions of this paper are as follows:

- For the first time, building on quantum circuit splitting, a novel distributed hybrid quantum convolutional neural network is proposed for the classification of medical images.
- A quantum convolutional neural network is introduced to enhance the model's understanding of both fine-grained and global features in medical images. High accuracy is achieved, and excellent performance is demonstrated.
- By employing quantum circuit splitting techniques, an 8-qubit QCNN can be expressed using only 5 qubits, nearly halving the required number of qubits. This approach significantly reduces the complexity of implementing quantum circuits while maintaining excellent performance.
- Compared to several recent models, our work achieves superior performance while utilizing fewer parameters.

The structure of this paper is organized as follows: related work is reviewed in section 2. A detailed description of the model architecture is provided in section 3. An evaluation of the performance of the model and comparisons with other networks are presented in section 4. Finally, the paper is concluded and future directions are discussed in section 5.

## 2. Related Works

### 2.1. CNN for medical image Classification

Convolutional neural networks, as a significant branch of deep learning, are utilized in medical image processing. CNN models such as GoogleNet (Szegedy et al. (2015)), AlexNet (Krizhevsky et al. (2017)), and Inception (Dong et al. (2020)) have been demonstrated to perform outstandingly in image classification and recognition tasks (Li et al. (2024)). In 2018, features were extracted using a pre-trained AlexNet and combined with an ECOC SVM classifier for skin cancer classification. In 2021, an automated network for brain tumor classification using SVM and CNN was proposed by Deepak and Ameer (2021). In 2023, a method that combines GoogleNet with the Dynamic Dipper Throated Optimization Algorithm (DDTPSO) for breast cancer classification was employed by Alhussan et al. (2023)

### 2.2. Quantum convolutional neural network

Recent successes in classical neural networks, coupled with advancements in quantum computing, have inspired the investigation of interactions between these technologies, culminating in the development of quantum neural networks.

The idea of quantum neural computation was first introduced by Kak (1995). In 2019, a physically realizable quantum convolutional neural network was introduced by Cong et al. (2019), resembling the structure of convolutional neural networks, with network layers constructed from parameterized quantum circuits. QCNNs were employed by Qu et al. (2023a) to extract features from medical images and integrate them with other modal features. In 2024, a custom convolutional neural network deep learning model was proposed by Rao et al. (2024), built on a quantum variational circuit with encoding, entanglement, and measurement capabilities.

Hybrid models have been proposed by researchers (Liu et al. (2021)), building on the strengths of both classical neural networks and quantum neural networks. In the work by Liang et al. (2021), a hybrid quantum-classical convolutional neural network is presented, which integrates residual block structures with quantum convolutional neural networks. In 2023, a hybrid quantum convolutional neural network was constructed by (Qu et al. (2023b)) to extract temporal features from electrocardiogram signals for detecting abnormal heartbeats.

Despite the rapid development of QCNNs, their application in medical image analysis remains limited. Therefore, designing a QCNN tailored for medical image classification is crucial.

### 2.3. Distributed quantum computing

Quantum computing for medical image classification is typically limited by qubit constraints due to hardware limitations. A promising solution to this challenge is distributed quantum computing (DQC), which offers greater feasibility and flexibility.

In 1993, DQC based on quantum teleportation was proposed by Bennett et al. (1993). In 2000, fault-tolerant quantum logic gates, were constructed by Zhou et al. (2000) from Stanford University using a method similar to quantum teleportation.

Among these, quantum circuit splitting is favored due to its ability to more accurately reconstruct quantum states and its broader applicability. In 2020, quantum circuit splitting was proposed and demonstrated by Peng et al. (2020). In 2022, quantum circuit splitting was utilized by Eddins et al. (2022) to express a  $2n$ -qubit quantum simulation as a linear combination of two  $n$ -qubit quantum simulations, effectively doubling the problem size that the chip can handle. In 2024, as described by Harrow and Lowe (2024), by employing quantum circuit splitting, involving the measurement of the existing quantum state and re-preparation based on the measurement results, facilitating the decomposition of the quantum circuit.

## 3. Method

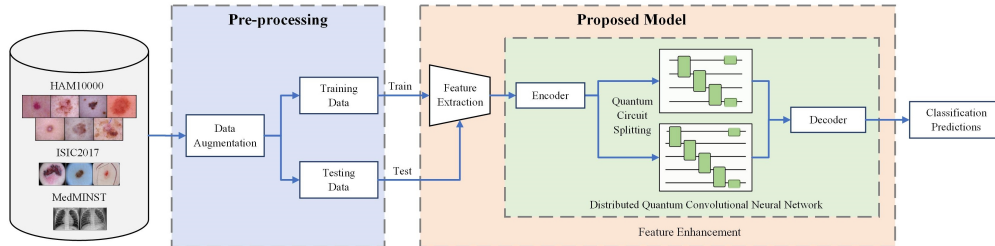


Figure 1: Complete workflow of medical image classification model

The execution flow of the system is illustrated in Figure 1. In the pre-processing phase, data augmentation and the division of the dataset into

training and testing sets are performed. The trained model is obtained using the training data, and the model’s performance is evaluated on the testing data based on classification predictions. The proposed model first employs a CNN for feature extraction and dimensionality reduction. The extracted feature vector is then used as input for a distributed 8-qubit quantum convolutional neural network. The 8-qubit quantum convolutional neural network employs the quantum circuit splitting technique, consisting of four groups, each formed by one 5-qubit QCNN and one 4-qubit QCNN. Finally, a fully connected layer is utilized for classification tasks. The framework of the proposed model is depicted in Figure 2.

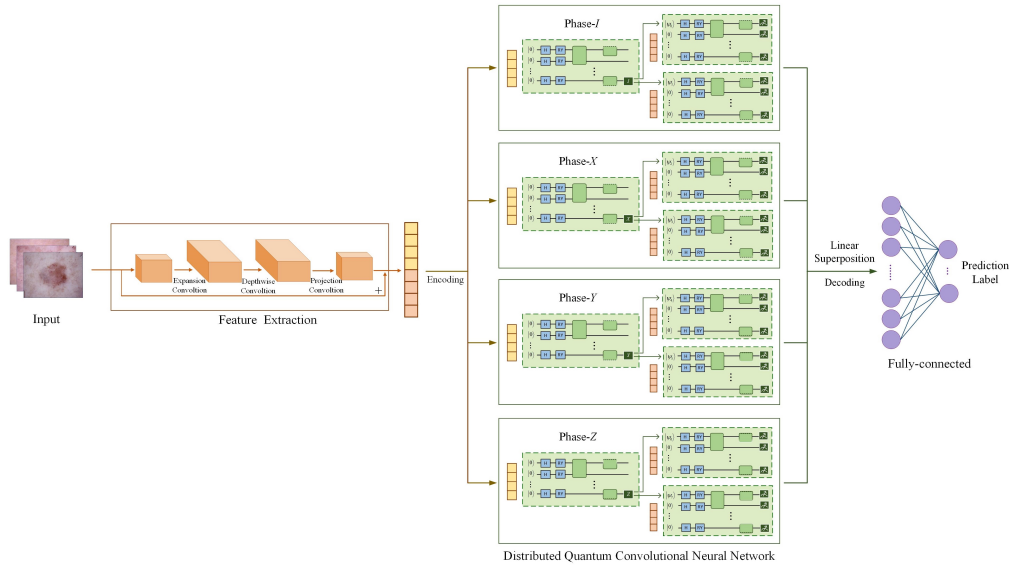


Figure 2: The framework of the proposed model

### 3.1. Feature extraction

A lightweight CNN architecture, MobileNetV2 Sandler et al. (2018), was employed to leverage its ability to capture spatial hierarchical features in images for medical image feature extraction. This network introduces ”Inverted Residuals and Linear Bottlenecks,” which implement an inverse residual structure opposite to that of traditional residual networks. Specifically, dimensions are first expanded through a  $1 \times 1$  convolution, followed by feature extraction via depthwise separable convolutions, and concluded with

another  $1 \times 1$  convolution for dimensionality reduction. Additionally, the concept of linear bottlenecks is incorporated into MobileNetV2, using linear transformations instead of nonlinear activation functions within the residual blocks. These bottleneck layers have fewer channels at both the input and output stages, while the intermediate expansion layers utilize lightweight depthwise convolutions to filter features. This approach significantly reduces computational demands and memory usage, further enhancing the model’s efficiency.

### 3.2. Quantum convolutional neural network

The learning task is enhanced by using a quantum convolutional neural network to extract high-dimensional features. The quantum convolutional neural network can be described using a quantum circuit. These circuits are composed of three main components: quantum state encoding, quantum entanglement layers, and quantum measurement. Quantum state encoding is responsible for loading data into the quantum system, with common encoding methods including basis state encoding, amplitude encoding, and angle encoding (Schuld (2018)). The quantum entanglement layer is employed for precise manipulation of quantum states, such as adjusting the rotation angle of quantum states via rotation gates. By arranging multiple quantum gates in a predetermined sequence, the initial quantum state can be transformed into the desired outcome. Finally, quantum measurement is used to extract classical information from the quantum state while effectively filtering out irrelevant information.

In our research, angle encoding is utilized to transform data from classical states into quantum states. Let  $D \subset R^n$  be a finite set, with each data point represented as  $x = (x_1, \dots, x_n) \in D$ . An injective function  $f$  is employed to map all subsets of  $D$  into a particular Hilbert space  $H^m$ , ensuring that for  $D' \subset D, f(D') \in H^m$ . For angle encoding, the relationship for any input  $D' = (x_0, x_1, \dots, x_{n-1})$  is defined as follows:

$$f(D') = \frac{1}{C} \sum_{i=1}^n x_i |i\rangle \tag{1}$$

The basis states of the qubits are represented by  $|i\rangle$ , indicating the different basis vectors of the quantum state. The normalization constant is given by  $C$ .

$$C = \sqrt{\sum_{i=1}^n x_i^2} \quad (2)$$

In quantum circuits, transformations are commonly achieved using the Hadamard gate ( $H$  gate) and the  $R_Y$  gate. The  $H$  gate is used to convert qubits from classical states to superposition states, while the  $R_Y$  gate is employed to rotate each qubit to the desired quantum state angle based on the input data values. The matrix representations are as follows:

$$H = \frac{1}{\sqrt{2}} \begin{bmatrix} 1 & 1 \\ 1 & -1 \end{bmatrix} \quad (3)$$

$$R_Y(\theta) = \exp\left(-i\frac{\theta}{2}Y\right) = \begin{bmatrix} \cos\left(\frac{\theta}{2}\right) & -\sin\left(\frac{\theta}{2}\right) \\ \sin\left(\frac{\theta}{2}\right) & \cos\left(\frac{\theta}{2}\right) \end{bmatrix} \quad (4)$$

In the quantum entanglement layer, a single-qubit gate ( $R_Z$ ) as well as two-qubit controlled rotation gates ( $CRY$  and  $CNOT$ ) are utilized. In these two-qubit gates, the control qubit is denoted by a black dot, while the target qubit is influenced by the associated operation. The matrix representations of these gates are presented as follows:

$$R_Z(\phi) = \begin{bmatrix} e^{-i\frac{\phi}{2}} & 0 \\ 0 & e^{i\frac{\phi}{2}} \end{bmatrix} \quad (5)$$

$$C(R_Y(\theta)) = \begin{bmatrix} I & 0 \\ 0 & R_Y(\theta) \end{bmatrix} \quad (6)$$

$$CNOT = \begin{bmatrix} 1 & 0 & 0 & 0 \\ 0 & 1 & 0 & 0 \\ 0 & 0 & 0 & 1 \\ 0 & 0 & 1 & 0 \end{bmatrix} \quad (7)$$

Inspired by CNNs, QCNNs are composed of convolutional layers and pooling layers. In the quantum convolutional layer, we employ a quasi-local unitary operator ( $U$ ) applied to the input quantum state in a translationally invariant manner. This approach allows for processing and feature extraction from the quantum state with limited depth, akin to the convolution operation



in classical convolutional neural networks. Consequently, the quantum convolutional network is able to effectively capture local features within quantum states while preserving the consistency of the global structure.

The quantum convolutional layer is designed with a matrix product states (MPS) structure. This structure is characterized by a ladder-like configuration that decomposes high-dimensional tensors into a series of lower-dimensional tensor products. These lower-rank tensors are interconnected through internal indices, referred to as the bond dimension  $D$ . The advantage of MPS lies in its ability to approximate complex quantum states with reduced computational complexity. Furthermore, by incorporating strong entanglement layers, the entanglement capabilities of MPS can be enhanced, thereby improving the performance of quantum circuits. Figure 3 illustrates the quantum circuit designed in this study. Each  $U$  in the MPS circuit is substituted with a simple variational quantum circuit, which represents the convolutional kernel, as illustrated in Figure 4. Subsequently, this circuit can be simulated, implemented on hardware, and optimized in the same manner as other variational quantum circuits.

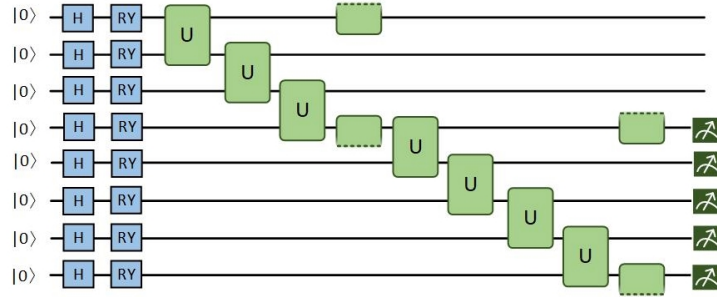


Figure 3: Structure of quantum circuit

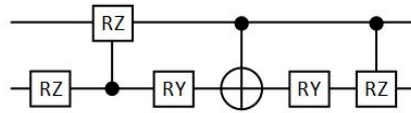


Figure 4: Quantum convolutional kernel

The design of quantum pooling layers aims to reduce the size of the feature map. However, after passing through our quantum convolutional layer, the

feature map size has become sufficiently small, allowing for the omission of the pooling layer.

The quantum state is converted into a classical state through measurement, with the results returned as a flat array containing the probabilities of measuring the computational basis states in the current configuration. If the measurement is constrained to  $N$  measurement circuits, the marginal probabilities can be obtained, resulting in a returned array size of  $2^n$ .

### 3.3. Quantum circuit splitting

The current quantum computing hardware is constrained by a limited number of qubits, finite quantum gate operation depths, and restricted connectivity between qubits, making it challenging for large-scale quantum circuits to be handled, particularly when the circuit size exceeds the hardware capabilities. By decomposing large circuits into a series of smaller circuits, more complex computational tasks can be performed on existing hardware.

In the process of quantum circuit splitting, a quantum splitting point is identified, allowing the circuit to be decomposed into two independent segments. To minimize the number of qubits involved, the cut is chosen to be performed in the middle of the quantum circuit. As illustrated in Figure 5, this approach decomposes an 8-qubit quantum circuit into a linear combination of a 4-qubit circuit and a 5-qubit circuit. By performing quantum tomography on the qubits before partitioning, one can learn the quantum state and reconstruct the inferred state in the partitioned qubits. Quantum tomography can be viewed as the process of expanding a quantum state and estimating coefficients in a specific basis, here chosen as the Pauli basis. By measuring the quantum state for each element in the basis, the quantum state prior to the cut can be reconstructed. Subsequently, by initializing the downstream qubits associated with the cut to the eigenstates of each element in the basis, the dynamic behavior of the circuit given the initial state can be learned. Ultimately, by reweighting the results obtained from multiple initializations, the overall behavior of the uncut circuit can be derived.

The quantum state at the splitting point in this paper can be expressed as follows:

$$\rho = U|q_3q_4q_5\rangle\langle q_3q_4q_5|U^\dagger \quad (8)$$

The unitary  $U$  is considered as arbitrary quantum gates, and  $U^\dagger$  is defined as the Hermitian conjugate of  $U$ . Once the qubit connections between the

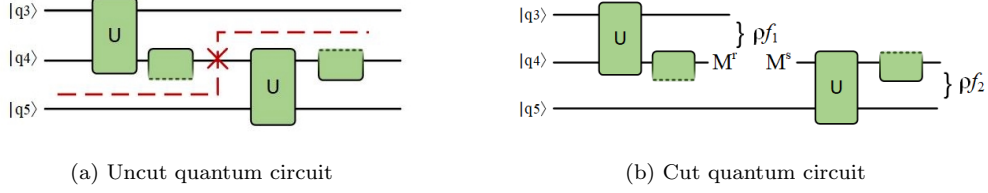


Figure 5: The quantum circuit diagram before and after cut

two unitary modules are severed, the equation can be rewritten as follows:

$$\rho = \frac{1}{2} \sum_{M \in \mathcal{B}} \rho_{f_1}(M) \otimes \rho_{f_2}(M) \quad (9)$$

$$\rho_{f_1}(M) = \text{Tr}(MU|q_3q_4\rangle\langle q_3q_4|U^\dagger) \quad (10)$$

$$\rho_{f_2}(M) = U(M \otimes |q_5\rangle\langle q_5|)U^\dagger \quad (11)$$

where  $M$  is the operator applied to the fourth qubit. Since the Pauli matrices are traceless operators, a spectral decomposition of  $M$  is necessary to obtain a physical interpretation. Equation 9 can then be rewritten as:

$$\rho = \frac{1}{2} \sum_{M \in \mathcal{B}} \sum_{r,s=\pm 1} r s \rho_{f_1}(M^r) \otimes \rho_{f_2}(M^s) \quad (12)$$

Here,  $r$  and  $s$  are denoted as the eigenvalues obtained from the spectral decomposition of the operator  $M$ , while  $M^r$  and  $M^s$  represent the corresponding eigenstates. The set  $\mathcal{B}$  encompasses the Pauli basis  $\{ I, X, Y, Z \}$ . The matrix representations of the Pauli operators are as follows:

$$\begin{aligned} I &= \begin{bmatrix} 1 & 0 \\ 0 & 1 \end{bmatrix} & X &= \begin{bmatrix} 0 & 1 \\ 1 & 0 \end{bmatrix} \\ Y &= \begin{bmatrix} 0 & -i \\ i & 0 \end{bmatrix} & Z &= \begin{bmatrix} 1 & 0 \\ 0 & -1 \end{bmatrix} \end{aligned} \quad (13)$$

The information transfer mechanism for the qubit-splitting line involves the measurement of the information stored in the 4th qubit during the computation process. This information is then initialized and transmitted to the remaining part of the circuit.

In a quantum circuit, any quantum operation represented by a unitary matrix  $U$  can be decomposed into a combination of orthogonal matrices formed by the Pauli basis.

$$U = \frac{\text{Tr}(UI)I + \text{Tr}(UX)X + \text{Tr}(UY)Y + \text{Tr}(UZ)Z}{2} \quad (14)$$

Based on the following spectral decomposition relationship, the Pauli basis can be rewritten as:

$$\begin{aligned} I &= |0\rangle\langle 0| + |1\rangle\langle 1| & X &= |+\rangle\langle +| - |-\rangle\langle -| \\ Y &= |+i\rangle\langle +i| - |-i\rangle\langle -i| & Z &= |0\rangle\langle 0| - |1\rangle\langle 1| \end{aligned} \quad (15)$$

Assuming  $O_i$  is represented as a Pauli matrix,  $\psi_i$  is denoted as the corresponding eigenstates, and  $2c_i$  signifies the associated eigenvalues, the following expression can be derived:

$$\begin{aligned} O_1 &= I, & \psi_1 &= |0\rangle\langle 0|, & c_1 &= +\frac{1}{2}; & O_2 &= I, & \psi_2 &= |1\rangle\langle 1|, & c_2 &= +\frac{1}{2}; \\ O_3 &= X, & \psi_3 &= |+\rangle\langle +|, & c_3 &= +\frac{1}{2}; & O_4 &= X, & \psi_4 &= |-\rangle\langle -|, & c_4 &= -\frac{1}{2}; \\ O_5 &= Y, & \psi_5 &= |+i\rangle\langle +i|, & c_5 &= +\frac{1}{2}; & O_6 &= Y, & \psi_6 &= |-i\rangle\langle -i|, & c_6 &= -\frac{1}{2}; \\ O_7 &= Z, & \psi_7 &= |0\rangle\langle 0|, & c_7 &= +\frac{1}{2}; & O_8 &= Z, & \psi_8 &= |1\rangle\langle 1|, & c_8 &= -\frac{1}{2}. \end{aligned} \quad (16)$$

From the above expression, it can be observed that an 8-qubit quantum circuit is decomposed into 8 groups, each comprising a 4-qubit circuit and a 5-qubit circuit. As illustrated in Equation 17, by performing a linear combination of these 8 pairs of dual quantum circuits, the original 8-qubit quantum circuit can be effectively reconstructed.

$$\langle q_4 \rangle = \sum_m^8 c_m (O_m \rho_m) \quad (17)$$

## 4. Experiments

### 4.1. Datasets and evaluation metrics

To train and evaluate the model, three publicly available datasets were utilized: HAM10000 dataset (Tschandl et al. (2018)), ISIC2017 dataset (Codella et al. (2018)) and MedMNIST (Yang et al. (2023)). The first and second

datasets are large-scale dermoscopic image multiclass datasets released by the International Skin Imaging Collaboration (ISIC) for the ISIC 2018 and 2017 competitions. The third dataset is the pneumonia dataset from MedMNIST, which consists of chest X-ray images for binary classification. The original information of the dataset is shown in Table 1.

Table 1: Datasets used in the experiments

Number	Dataset	Categories/Count	Total	Size
1	HAM10000	AK: 327	10015	$450 \times 600$
		BCC: 514		
		BKL: 1099		
		DF: 115		
		MEL: 1113		
		NV: 6705		
		VASC: 142		
2	ISIC2017	BKL: 254	2000	$767 \times 1022$
		MEL: 374		
		NV: 1372		
3	MedMNIST	NL: 1583	5856	$224 \times 224$
		PNA: 4273		

To address the imbalance in dermoscopic image, data augmentation was applied to the first and second datasets, resulting in 1,372 and 2,000 images for each class, respectively. Additionally, data of varying sizes were normalized and cropped to a uniform size of  $224 \times 224$  pixels to ensure consistency and comparability.

Multiple evaluation metrics were employed to quantify the performance of the experimental results, including AUC, accuracy, recall, precision, f1-score, and specificity (Wu et al. (2022)). From a clinical perspective, recall and specificity are important because they directly influence accurate identification and exclusion, thereby impacting precise diagnosis and effective patient management.

#### 4.2. Experimental setup

In our study, the computational resources were comprised of four NVIDIA GeForce RTX 4090 GPUs, a 192-core Intel CPU, and 128 GB of memory. The model was implemented on the CUDA 12.0 platform using the PyTorch and PennyLane frameworks.

In addition to the MedMNIST dataset, which is divided into an 8:1:1 ratio, other datasets are typically split into training and testing sets with an 8:2 ratio. During the model training phase, we use an Adadelta optimizer with the learning rate of 0.05. We use cross-entropy loss and set the batch size as 16.

### 4.3. Experimental Results

#### 4.3.1. Performance evaluation on the HAM10000

The model’s 7-class classification performance on the HAM10000 dataset is presented in Table 2. Among all categories, the best performance was demonstrated in DF (dermatofibroma), with a specificity of 99.92% and both precision and f1-score of 99.47%. For VASC (vascular lesions), the highest recall of 100% was attained, with specificity, precision, and f1-score all exceeding 98%. However, the recall for NV (nevus) was relatively low, at only 75.59%. In Figure 6, the confusion matrix for the HAM10000 dataset is shown. It is revealed through analysis that some NV samples were misclassified as MEL (melanoma). Overall, we achieved an accuracy of 91.14% on this dataset, demonstrating that the model can perform exceptionally well in multi-class problems, such as the 7-class classification task.

Table 2: Performance on HAM10000

Categories	Specificity	Precision	Recall	F1-score
AK	98.65%	93.10%	99.54%	96.21%
BCC	98.95%	94.00%	96.08%	95.03%
BKL	97.74%	86.40%	83.45%	84.90%
DF	<b>99.92%</b>	<b>99.47%</b>	99.47%	<b>99.47%</b>
MEL	96.49%	80.05%	83.42%	81.70%
NV	98.10%	86.23%	75.59%	80.56%
VASC	99.79%	98.71%	<b>100%</b>	99.35%

#### 4.3.2. Performance evaluation on the ISIC2017

The model’s 3-class classification performance on the ISIC2017 dataset is presented in Table 3. Among the categories, the best performance was observed for NV, with a recall of 100%, precision of 97.31%, and f1-score of 98.63%, the highest across all categories. In comparison, MEL (melanoma) achieved a specificity of 98.73%, but its recall was relatively lower at 85.98%.

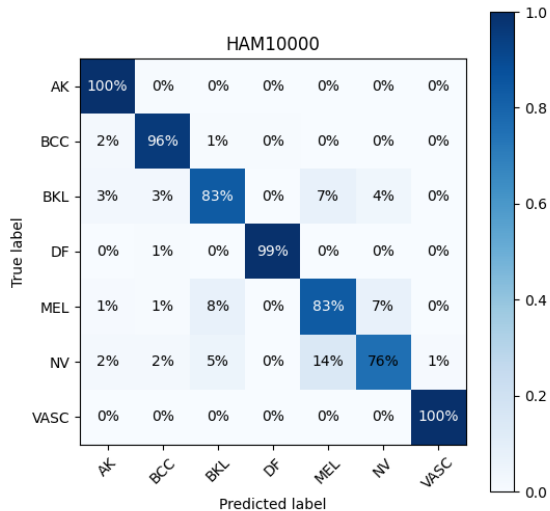


Figure 6: The confusion matrix of the HAM10000

Furthermore, the precision for BKL (seborrheic) was below 90%. As shown in the confusion matrix in Figure 7, the prediction accuracy for MEL was 86%, with 11% of the samples misclassified as BKL. An overall classification accuracy of 94.54% was achieved. Our model demonstrates excellent classification performance, in the context of a three-class classification task.

Table 3: Performances on ISIC2017

Categories	Specificity	Precision	Recall	F1-score
BKL	94.64%	89.55%	97.35%	93.28%
MEL	<b>98.73%</b>	97.08%	85.98%	91.19%
NV	98.50%	<b>97.31%</b>	<b>100%</b>	<b>98.63%</b>

#### 4.3.3. Performance evaluation on the MedMNIST

The results of the model’s binary classification task on the MedMNIST dataset are shown in Table 4. In the category NL (normal), the specificity and precision are highest, at 97.94% and 96.69%, respectively. However, recall and f1-score are surpassed by the category PNA (Pneumonia).

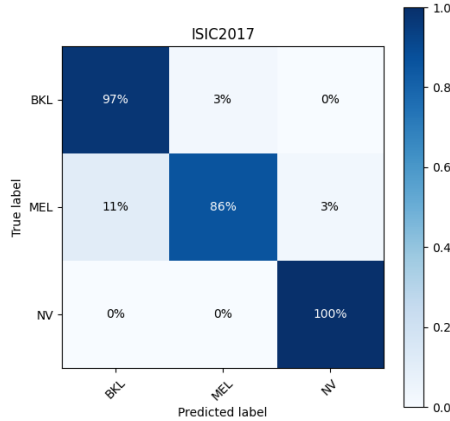


Figure 7: The confusion matrix of the ISIC2017

This discrepancy is due to the imbalance in the dataset, where the number of pneumonia cases significantly exceeds that of normal cases, leading to a decline in certain metrics.

In benchmark experiments, as shown in Table 5 our model achieved the highest ACC and the second-highest AUC. This demonstrates that our model exhibits a very high correct diagnosis rate for binary classification tasks involving pneumonia.

Table 4: Performances on MedMNIST

Categories	Specificity	Precision	Recall	F1-score
NL	<b>97.94%</b>	<b>96.69%</b>	74.79%	84.34%
PNA	76.77%	86.68%	<b>98.46%</b>	<b>92.20%</b>

#### 4.3.4. Comparison experiments and analysis

Our model was compared with existing models, and the results are presented. These models include CNNs such as ResNet34 (He et al. (2016)), DenseNet121 (Huang et al. (2017)), VGG16+SA (Gao (2021)), and QCNNs such as Qst-Cla (Ahmed et al. (2021)), HQCNN (Yadav et al. (2023)), and HQNN-Parallel (Senokosov et al. (2024)). The same dataset split method and a similar training strategy were used to perform comparisons between these



Table 5: Benchmark on MedMNIST

Model	ACC	AUC
ResNet-18	86.43%	<b>95.55%</b>
auto-sklearn	85.53%	94.18%
classical AutoKeras	87.76%	94.72%
<b>our work</b>	<b>89.58%</b>	94.87%

Table 6: Performance comparison on HAM10000

Dataset	Model	Accuracy(%)	Specificity(%)	Precision(%)	Recall(%)	F1-score(%)	Para (M)
HAM10000	ResNet34(He et al. (2016))	89.35	99.71	89.18	89.33	89.14	20.32
	DenseNet121(Huang et al. (2017))	89.50	<b>99.92</b>	89.44	89.50	89.33	6.72
	VGG16+SA(Gao (2021))	85.53	99.46	86.00	85.42	85.49	45.75
	Qst-Cla(Ahmed et al. (2021))	87.92	99.71	88.79	87.67	87.23	78.23
	HQCNN(Yadav et al. (2023))	73.32	98.92	75.07	73.75	72.98	84.01
	HQNN-Parallel(Senokosov et al. (2024))	82.39	98.96	83.45	82.32	82.02	11.50
	<b>Our work</b>	<b>91.14</b>	99.63	<b>91.14</b>	<b>91.09</b>	<b>91.03</b>	<b>2.16</b>

models on two medical image datasets related to skin cancer, HAM10000 and ISIC2017. The results demonstrate that excellent performance was achieved by our designed model on both datasets.

On the HAM10000 dataset (Table 6), an accuracy of 91.14% was demonstrated by our model, surpassing other models. In terms of specificity, nearly 100% was achieved, indicating exceptional performance in identifying negative class samples. Both precision and recall exceeded 91%, further highlighting the model’s strong stability in recognizing positive class samples. In comparison, other hybrid quantum models such as Qst-Cla and HQCNN, did not achieve performance metrics above 90% except for specificity.

On the ISIC2017 dataset (Table 7), an accuracy of 94.54% was reached by our model, significantly outperforming other CNNs such as ResNet34 (90.53%), DenseNet121 (88.47%), and VGG16+SA (88.59%). This high

Table 7: Performance comparison on ISIC2017

Dataset	Model	Accuracy(%)	Specificity(%)	Precision(%)	Recall(%)	F1-score(%)	Para (M)
ISIC2017	ResNet34(He et al. (2016))	90.53	96.64	90.38	90.37	90.29	20.32
	DenseNet121(Huang et al. (2017))	88.47	93.83	88.76	88.29	87.98	6.71
	VGG16+SA(Gao (2021))	88.59	96.26	88.45	88.49	88.39	45.73
	Qst-Cla(Ahmed et al. (2021))	80.46	89.91	81.47	80.12	78.78	78.23
	HQCNN (Yadav et al. (2023))	81.31	96.82	81.22	81.06	81.13	84.01
	HQNN-Parallel(Senokosov et al. (2024))	79.24	88.59	79.47	78.90	78.02	11.50
	<b>Our work</b>	<b>94.54</b>	<b>98.50</b>	<b>94.65</b>	<b>94.44</b>	<b>94.37</b>	<b>2.16</b>

accuracy reflects the outstanding overall classification performance of the model, as well as its advantage in extracting complex image features. Additionally, a specificity of 98.50% was achieved, showcasing exceptional ability in identifying negative class samples. In the evaluation of precision and recall, 94.65% and 94.44% were attained, respectively, with an f1-score of 94.37%. These metrics indicate strong performance in identifying positive class samples. In comparison, other quantum models, such as HQCNN and HQNN-Parallel, were outperformed, achieving accuracies of 81.31% and 79.24%, respectively. This difference may be attributed to the complexity of their network structures. In contrast, our network structure are simpler and more effective.

Furthermore, in terms of number of parameters, only 2.16M parameters are contained in our model, which is significantly smaller than other models. While maintaining outstanding performance, significant model size compression has been achieved, making it especially suitable for resource-limited medical imaging tasks. This demonstrates that excellent performance can still be achieved in resource-constrained environments.

#### 4.3.5. Ablation experiments and analysis

To evaluate the impact of the quantum circuit splitting technique on the model, ablation experiments were conducted on both medical datasets, HAM10000 and ISIC2017, as shown in Table 8. After adopting distributed computing based on quantum circuit splitting, our model shows an improvement of approximately 2%-3% in various metrics. This indicates that the introduction of quantum circuit splitting not only overcomes hardware limitations and reduces the required theoretical quantum bits but also enhances the model’s learning capability. This experiment strongly demonstrates the feasibility of the quantum circuit splitting.

Table 8: Ablation study results

Dataset	Cut	Accuracy	Specificity	Precision	Recall	F1-score
HAM10000	×	89.57%	99.65%	89.75%	89.59%	89.50%
	✓	<b>91.14%</b>	<b>99.73%</b>	<b>91.14%</b>	<b>91.09%</b>	<b>91.03%</b>
ISIC2017	×	91.26%	98.13%	91.26%	91.20%	91.11%
	✓	<b>94.54%</b>	<b>98.50%</b>	<b>94.65%</b>	<b>94.44%</b>	<b>94.37%</b>

## 5. Conclusions and Future Work

In this paper, a novel distributed hybrid quantum convolutional neural network is presented for the classification of medical images. A quantum convolutional neural network is designed, leveraging the advantages of quantum computing to explore a broader parameter space. In the context of limited quantum hardware resources, quantum circuit splitting is introduced into the quantum circuit, where the 8-qubit quantum circuit is split into two separate circuits, one 4-qubit and the other 5-qubit, significantly reducing quantum resource usage. The performance of medical image classification networks is improved by our hybrid quantum convolutional neural network, and the combination of a lightweight classical network and scalable quantum circuits greatly reduces the parameter count and saves computational resources. Compared to other CNNs, our work maintains high performance while expanding into the promising domain of quantum computing. When compared to other QCNNs, higher accuracy is achieved by our proposed method, making it more feasible for practical applications.

In future research, we will explore the optimization potential of this model across additional datasets and tasks. The model will be optimized by closely integrating deep learning with parameterized quantum circuits, using fewer quantum bits to simulate larger-scale quantum circuits. Additionally, its application will be extended to tasks beyond image classification.

### **CRedit authorship contribution statement**

**Yangyang Li:** Validation, Supervision, Methodology, Conceptualization. **Zhengya Qi:** Writing – review & editing, Writing – original draft, Formal analysis. **Yuelin Li:** Writing – review & editing, Formal analysis. **Haorui Yang:** Writing – review & editing, Data curation. **Ronghua Shang:** Investigation. **Licheng Jiao:** Investigation.

### **Declaration of competing interest**

The authors declare that they have no known competing financial interests or personal relationships that could have appeared to influence the work reported in this paper.

## Acknowledgments

This work was supported in part by the National Natural Science Foundation of China under Grant 62476209, in part by the Key Research and Development Program of Shaanxi under Grant 2024CY2-GJHX-18, and in part by the Natural Science Basic Research Program of Shaanxi under Grant No.2022JC-45.

## References

- Ahmed, S., Sánchez Muñoz, C., Nori, F., Kockum, A.F., 2021. Classification and reconstruction of optical quantum states with deep neural networks. *Physical Review Research* 3, 033278.
- Albahri, O., Zaidan, A., Albahri, A., Zaidan, B., Abdulkareem, K.H., Alqaysi, Z., Alamoodi, A., Aleesa, A., Chyad, M., Alesa, R., Lim, C., Lakulu, M.M., Ibrahim, A., Rashid, N.A., 2020. Systematic review of artificial intelligence techniques in the detection and classification of covid-19 medical images in terms of evaluation and benchmarking: Taxonomy analysis, challenges, future solutions and methodological aspects. *Journal of Infection and Public Health* 13, 1381–1396.
- Alhussan, A.A., Eid, M.M., Towfek, S., Khafaga, D.S., 2023. Breast cancer classification depends on the dynamic dipper throated optimization algorithm. *Biomimetics* 8, 163.
- Bennett, C.H., Brassard, G., Crépeau, C., Jozsa, R., Peres, A., Wootters, W.K., 1993. Teleporting an unknown quantum state via dual classical and einstein-podolsky-rosen channels. *Physical Review Letters* 70, 1895.
- Codella, N.C.F., Gutman, D., Celebi, M.E., Helba, B., Marchetti, M.A., Dusza, S.W., Kalloo, A., Liopyris, K., Mishra, N., Kittler, H., Halpern, A., 2018. Skin lesion analysis toward melanoma detection: A challenge at the 2017 international symposium on biomedical imaging (isbi), hosted by the international skin imaging collaboration (isic), in: 2018 IEEE 15th International Symposium on Biomedical Imaging (ISBI 2018), IEEE. pp. 168–172.
- Cong, I., Choi, S., Lukin, M.D., 2019. Quantum convolutional neural networks. *Nature Physics* 15, 1273–1278.

- De Leon, N.P., Itoh, K.M., Kim, D., Mehta, K.K., Northup, T.E., Paik, H., Palmer, B., Samarth, N., Sangtawesin, S., Steuerman, D.W., 2021. Materials challenges and opportunities for quantum computing hardware. *Science* 372, eabb2823.
- Deepak, S., Ameer, P., 2021. Automated categorization of brain tumor from mri using cnn features and svm. *Journal of Ambient Intelligence and Humanized Computing* 12, 8357–8369.
- Ding, S., Wu, Z., Zheng, Y., Liu, Z., Yang, X., Yang, X., Yuan, G., Xie, J., 2021. Deep attention branch networks for skin lesion classification. *Computer Methods and Programs in Biomedicine* 212, 106447.
- Dong, N., Zhao, L., Wu, C.H., Chang, J.F., 2020. Inception v3 based cervical cell classification combined with artificially extracted features. *Applied Soft Computing* 93, 106311.
- Dorj, U.O., Lee, K.K., Choi, J.Y., Lee, M., 2018. The skin cancer classification using deep convolutional neural network. *Multimedia Tools and Applications* 77, 9909–9924.
- Eddins, A., Motta, M., Gujarati, T.P., Bravyi, S., Mezzacapo, A., Hadfield, C., Sheldon, S., 2022. Doubling the size of quantum simulators by entanglement forging. *PRX Quantum* 3, 010309.
- Gao, M., 2021. Soft attention improves skin cancer classification performance. *Interpretability of Machine Intelligence in Medical Image Computing, and Topological Data Analysis and Its Applications for Medical Data* 12929, 13.
- Giaquinto, A.N., Sung, H., Miller, K.D., Kramer, J.L., Newman, L.A., Minihan, A., Jemal, A., Siegel, R.L., 2022. Breast cancer statistics, 2022. *CA: A Cancer Journal for Clinicians* 72, 524–541.
- Harrow, A.W., Lowe, A., 2024. Optimal quantum circuit cuts with application to clustered hamiltonian simulation. *arXiv preprint arXiv:2403.01018*.
- He, K., Zhang, X., Ren, S., Sun, J., 2016. Deep residual learning for image recognition, in: *Proceedings of the IEEE Conference on Computer Vision and Pattern Recognition (CVPR)*, IEEE. pp. 770–778.

- Houssein, E.H., Abohashima, Z., Elhoseny, M., Mohamed, W.M., 2022. Hybrid quantum-classical convolutional neural network model for covid-19 prediction using chest x-ray images. *Journal of Computational Design and Engineering* 9, 343–363.
- Huang, G., Liu, Z., Van Der Maaten, L., Weinberger, K.Q., 2017. Densely connected convolutional networks, in: *Proceedings of the IEEE Conference on Computer Vision and Pattern Recognition (CVPR)*, IEEE. pp. 4700–4708.
- Jiwani, N., Gupta, K., Afreen, N., 2022. A convolutional neural network approach for diabetic retinopathy classification, in: *2022 IEEE 11th International Conference on Communication Systems and Network Technologies (CSNT)*, IEEE. pp. 357–361.
- Kak, S.C., 1995. Quantum neural computing. *Advances in Imaging and Electron Physics* 94, 259–313.
- Karthik, R., Vaichole, T.S., Kulkarni, S.K., Yadav, O., Khan, F., 2022. Eff2net: An efficient channel attention-based convolutional neural network for skin disease classification. *Biomedical Signal Processing and Control* 73, 103406.
- Kaur, T., Gandhi, T.K., 2019. Automated brain image classification based on vgg-16 and transfer learning, in: *2019 international conference on information technology (ICIT)*, IEEE. pp. 94–98.
- Klimov, P., Kelly, J., Chen, Z., Neeley, M., Megrant, A., Burkett, B., Barends, R., Arya, K., Chiaro, B., Chen, Y., et al., 2018. Fluctuations of energy-relaxation times in superconducting qubits. *Physical Review Letters* 121, 090502.
- Krizhevsky, A., Sutskever, I., Hinton, G.E., 2017. Imagenet classification with deep convolutional neural networks. *Communications of the ACM* 60, 84–90.
- Li, Y., Li, Y., Zhang, S., Liu, G., Chen, Y., Shang, R., Jiao, L., 2024. An attention-based, context-aware multimodal fusion method for sarcasm detection using inter-modality inconsistency. *Knowledge-Based Systems* 287, 111457.

- Li, Y., Liu, R., Hao, X., Shang, R., Zhao, P., Jiao, L., 2023. Eqnas: Evolutionary quantum neural architecture search for image classification. *Neural Networks* 168, 471–483.
- Liang, Y., Peng, W., Zheng, Z.J., Silvén, O., Zhao, G., 2021. A hybrid quantum–classical neural network with deep residual learning. *Neural Networks* 143, 133–147.
- Liu, J., Lim, K.H., Wood, K.L., Huang, W., Guo, C., Huang, H.L., 2021. Hybrid quantum-classical convolutional neural networks. *Science China Physics, Mechanics & Astronomy* 64, 290311.
- Panchi, L., Shiyong, L., 2008. Learning algorithm and application of quantum bp neural networks based on universal quantum gates. *Journal of Systems Engineering and Electronics* 19, 167–174.
- Peng, T., Harrow, A.W., Ozols, M., Wu, X., 2020. Simulating large quantum circuits on a small quantum computer. *Physical Review Letters* 125, 150504.
- Qu, Z., Li, Y., Tiwari, P., 2023a. Qnmf: A quantum neural network based multimodal fusion system for intelligent diagnosis. *Information Fusion* 100, 101913.
- Qu, Z., Shi, W., Liu, B., Gupta, D., Tiwari, P., 2023b. Iomt-based smart healthcare detection system driven by quantum blockchain and quantum neural network. *IEEE Journal of Biomedical and Health Informatics* 28, 3317–3328.
- Rao, G.E., Rajitha, B., Srinivasu, P.N., Ijaz, M.F., Woźniak, M., 2024. Hybrid framework for respiratory lung diseases detection based on classical cnn and quantum classifiers from chest x-rays. *Biomedical Signal Processing and Control* 88, 105567.
- Sandler, M., Howard, A., Zhu, M., Zhmoginov, A., Chen, L.C., 2018. Mobilenetv2: Inverted residuals and linear bottlenecks, in: *Proceedings of the IEEE conference on computer vision and pattern recognition (CVPR)*, IEEE. pp. 4510–4520.
- Schuld, M., 2018. *Supervised learning with quantum computers*. Springer.

- Schuld, M., Fingerhuth, M., Petruccione, F., 2017. Implementing a distance-based classifier with a quantum interference circuit. *Europhysics Letters* 119, 60002.
- Senokosov, A., Sedykh, A., Sagingalieva, A., Kyriacou, B., Melnikov, A., 2024. Quantum machine learning for image classification. *Machine Learning: Science and Technology* 5, 015040.
- Smith, K.N., Ravi, G.S., Baker, J.M., Chong, F.T., 2022. Scaling superconducting quantum computers with chiplet architectures, in: 2022 55th IEEE/ACM International Symposium on Microarchitecture (MICRO), IEEE. pp. 1092–1109.
- Sulthana, R., Chamola, V., Hussain, Z., Albalwy, F., Hussain, A., 2024. A novel end-to-end deep convolutional neural network based skin lesion classification framework. *Expert Systems with Applications* 246, 123056.
- Szegedy, C., Liu, W., Jia, Y., Sermanet, P., Reed, S., Anguelov, D., Erhan, D., Vanhoucke, V., Rabinovich, A., 2015. Going deeper with convolutions, in: 2015 IEEE Conference on Computer Vision and Pattern Recognition (CVPR), IEEE. pp. 1–9.
- Tang, W., Tomesh, T., Suchara, M., Larson, J., Martonosi, M., 2021. Cutqc: using small quantum computers for large quantum circuit evaluations, in: Proceedings of the 26th ACM International conference on architectural support for programming languages and operating systems, Association for Computing Machinery. pp. 473–486.
- Tian, J., Sun, X., Du, Y., Zhao, S., Liu, Q., Zhang, K., Yi, W., Huang, W., Wang, C., Wu, X., et al., 2023. Recent advances for quantum neural networks in generative learning. *IEEE Transactions on Pattern Analysis and Machine Intelligence* 45, 12321–12340.
- Tschandl, P., Rosendahl, C., Kittler, H., 2018. The ham10000 dataset, a large collection of multi-source dermatoscopic images of common pigmented skin lesions. *Scientific Data* 5, 1–9.
- Wu, Y., Chen, B., Zeng, A., Pan, D., Wang, R., Zhao, S., 2022. Skin cancer classification with deep learning: a systematic review. *Frontiers in Oncology* 12, 893972.



- Yadav, A., Sridevi, S., Balachandran, S., et al., 2023. Hybrid quantum-classical convolutional neural network for allen telescope seti image classification, in: 2023 14th International Conference on Computing Communication and Networking Technologies (ICCCNT), IEEE. pp. 1–6.
- Yang, J., Shi, R., Wei, D., Liu, Z., Zhao, L., Ke, B., Pfister, H., Ni, B., 2023. Medmnist v2-a large-scale lightweight benchmark for 2d and 3d biomedical image classification. *Scientific Data* 10, 41.
- Zhou, X., Leung, D.W., Chuang, I.L., 2000. Methodology for quantum logic gate construction. *Physical Review A* 62, 052316.